

Application of Doppler spectroscopy in H₂ to the prediction of experimental D(*d,n*)³He reaction rates in an inertial electrostatic confinement device

J. Kipritidis* and J. Khachan

School of Physics, University of Sydney, Sydney, Australia 2006

(Received 30 July 2008; revised manuscript received 24 September 2008; published 4 February 2009)

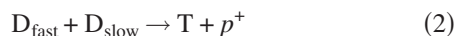
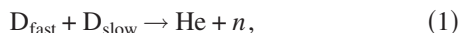
In our previous paper, we developed an optical measurement for absolute densities of fast (tens of keV) H ions in an abnormal hollow cathode discharge of hydrogen in the units to tens of mTorr pressure range. We apply this method to a cylindrically symmetric inertial electrostatic confinement (IEC) discharge of hydrogen using the Doppler spectrum of H_α. We predict neutron production rates for an equivalent discharge of deuterium and compare these with experimental values under the separate conditions of constant deuterium gas pressure (~6 mTorr) and voltage (30 kV). Our predictions capture the variation of production rates with dc current (10–50 mA) and agree with experiment to within an order of magnitude. The applicability of this diagnostic to the cylindrical IEC discharge is thus demonstrated, with our results supporting the theory that the discharge is dominated by energetic neutrals emerging from the cathode apertures.

DOI: [10.1103/PhysRevE.79.026403](https://doi.org/10.1103/PhysRevE.79.026403)

PACS number(s): 52.59.-f, 52.70.-m, 32.30.-r, 32.70.Fw

I. INTRODUCTION

Inertial electrostatic confinement (IEC) fusion has long been presented as a relatively simple means for producing controlled nuclear fusion reactions, but there has been surprisingly little emphasis on the application of optical diagnostics in characterizing the IEC discharge. Figure 1 depicts one configuration, with an open-ended and cylindrically symmetric cathode sitting within a grounded cylindrical chamber (anode). In the conventional picture [1] of a deuterium-filled device, most energetic or “fast” (tens of keV) deuterons are produced by fast electrons in the inter-electrode region and accelerate towards the cathode. Explicitly, the scheme aims to produce nuclear fusion within the cathode center between converging populations of fast, monoenergetic deuterons D_{fast}. Both in simulation and experiment however [2], the majority of fusion occurs with a low-energy deuteron D_{slow} associated with a “cold” background gas (temperature T_{gas}=300 K) through the following reactions:



of which approximately half produce a neutron of energy ~2.45 MeV and a helium nucleus, with the other half producing a proton and tritium. The maximum interaction cross section $\sigma_{\text{D-D}}$ for the D-D fusion process is $\sim 1 \times 10^{-29} \text{ m}^2$, occurring for a projectile energy around 2 MeV. Historically, the characterization of energetic particle densities in terms of operating parameters and electrode design involved measuring neutron production rates directly (for example, in this work through the scintillation-detection of nuclear fission in a Li-I crystal placed near the IEC device). With recent devices aiming to pulse the cathode voltage as high as 300 kV with instantaneous neutron production rates in excess of 10^{11} s^{-1} , such detection methods requires particular consid-

eration towards radiation shielding. Moreover deuterium may be expensive to procure in pure gaseous form. In this work, we aim to demonstrate the utility of an optical method for predicting fusion rates in a deuterium-filled IEC device—without neutron production and without the need for deuterium gas—by performing Doppler spectroscopy on a similar discharge of hydrogen.

In Ref. [3] we developed an optical measurement for the absolute densities of fast H ions in the vicinity of the cathode edge for a hydrogen-filled IEC at units of mTorr pressures. Calculation requires only two inputs—the current density due to fast electrons and a single spectrum of H_α (the radiative atomic transition corresponding to principal quantum number $n=3 \rightarrow 2$) measured several centimeters away from the cathode, with spectroscopy being convenient due to collimated channels of brilliant optical emission emerging from the cathode apertures [4–6].

The typical H_α line shape consists of a central Lorentzian peak (with an intensity maximum at wavelength λ_0

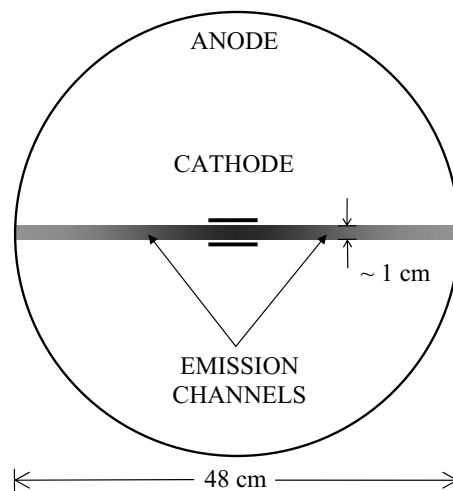


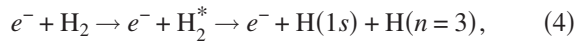
FIG. 1. Schematic diagram of an IEC discharge in the “abnormal hollow cathode” mode. The anode is a closed and grounded cylindrical chamber, the cathode an open-ended cylinder of stainless steel.

*johnk@physics.usyd.edu.au

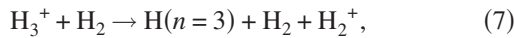
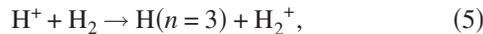
$\sim 6563 \text{ \AA}$) flanked by Gaussian-like, Doppler-shifted wings. The kinetic energy K of an emitting neutral is related to the Doppler shift $\Delta\lambda$ of emission through

$$K = \frac{mc^2(\Delta\lambda)^2}{2\lambda_0^2 \cos^2 \theta}, \quad (3)$$

where m is the particle mass, c is the speed of light, and θ is the angle between the particle trajectory and observation axis. Our spectroscopic method makes three assumptions with regards to the spectrum. The first is that Doppler shift magnitudes smaller than 0.3 \AA may be attributed to dissociative excitation (see Sec. IV A of Ref. [7]) of ground state H_2 by fast electrons which are approximately monoenergetic [8],



with the primary deexcitation mechanism being spontaneous emission. The second is that the far wings (“energetic” Doppler peaks with $\Delta\lambda \gtrsim 3 \text{ \AA}$) arise primarily through the charge exchange of fast ion species H_x^+ (for $x=1-3$) with the background gas. For the mTorr pressure range the dominant reactions are



with each product $\text{H}(n=3)$ possessing the same trajectory as the incident ion and a fraction $1/x$ of its incident kinetic energy [9]. Doppler peak positions thus characterize the energies and trajectories of incident ions, with an increase in wavelength (“redshift”) being indicative of particles emitting as they travel away from the detector. The third assumption is that we may equate the measured cathode current to that of fast electrons in the beam, introducing a $1/r_e^2$ dependence of electron density on electron beam radius r_e (see Sec. III A).

The result is a simple expression relating intensity ratios of Doppler and central peaks measured at the anode (several centimeters away from the cathode at an angle $\theta < 90^\circ$ to the beam), to the density ratio of fast electrons at the anode and fast H_x^+ exiting the corresponding cathode aperture. The key output of this calculation is the dissociation fraction f_{fast} of the background gas into energetic ions at the cathode edge. The expression is detailed in Sec. III A along with an expression for using measured values of f_{fast} in the prediction of neutron production rates by process (1) for an “equivalent discharge” (same cathode current and voltage) of D_2 . Explicitly, the calculated $\text{D}(d,n)^3\text{He}$ reaction rate is proportional to f_{fast} and the square of the neutral beam radius r_n .

We note that for the present configuration and plasma parameters (voltages 10–30 kV, current 10–50 mA, and pressures 1–10 mTorr in H_2), voltage is observed to rise as the logarithm of current. Figure 2 depicts a typical voltage-current curve for steady-state dc operation, which we have termed an “abnormal hollow cathode discharge.” In justifying this terminology, we note that the cathode geometry is reminiscent of hollow cathode spectral lamps with the important difference that the present discharge operates at pres-

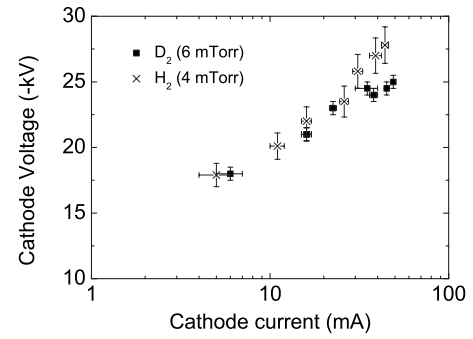


FIG. 2. Voltage versus current curves in H_2 (4 mTorr) and D_2 (6 mTorr) for the IEC apparatus described in Sec. II.

ures at least an order of magnitude lower; the cathode interior is no longer a region of intrinsically efficient ionization as the mean free path for ionization by electrons is at least an order of magnitude larger than the dimensions of the cathode itself. Moreover the voltage-current relation in Fig. 2 resembles the “abnormal glow” between plane parallel electrodes where cathode current exceeds the product of cathode surface area and normal glow current density. This is consistent with the observation that it is the intensity of the emission channels (as opposed to their radii) which undergoes the most marked increase over this current range.

For a cylindrical IEC discharge of H_2 operating in the abnormal hollow cathode mode at units and tens of mTorr, the observed Doppler spectra are consistent with the interpretation that the emission channels are dominated by fast neutrals which are produced within the cathode interior and emerge from the cathode apertures [10,11]. This has been linked to Langmuir probe measurements of a positive space charge or “virtual anode” at the center of a similar (two-ring) cathode geometry [5], as well as dusty plasma experiments [12] which indicate that the dominant flow of ions within the cathode is away from the cathode center. Along the beam axis, the potential field resembles a double-parabolic well, with each parabola centered at the cathode apertures. The height of the potential “hump” at the center has been routinely inferred as being in the order 30–50 % of the potential applied to the cathode. The implication is that at least some significant fraction of the energetic neutrals emerging from the cathode apertures are produced by ions undergoing charge exchange within the cathode as they accelerate away from the virtual anode. Paradoxically, the virtual anode itself is thought to arise in part due to ions produced in the inter-electrode space by fast electrons and accelerating toward the cathode center. It is anticipated that measurement of the fast neutral densities may assist in future modeling of this complex interplay between “converging” and “diverging” ion species.

In this paper, we demonstrate the applicability of our optical diagnostic for fast ion densities in H_2 to the prediction of absolute neutron production rates for the separate conditions of constant pressure (6 mTorr) and voltage (–30 kV) in D_2 . Our IEC system, as well as the apparatus and calibrations used for these two independent methods are described in Sec. II. In Sec. III we review the theory for the optical diagnostic, and in Sec. IV we suggest how the agreement be-

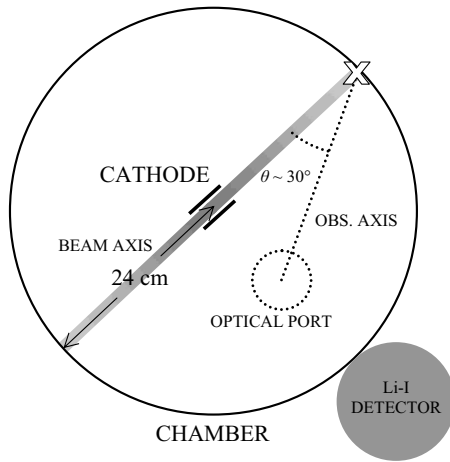


FIG. 3. Top-down schematic of the electrode arrangement and other apparatus components used in this study. See text for explanation.

tween predicted and measured fusion rates may provide support for the theory that the discharge is dominated by energetic neutrals.

II. EXPERIMENTAL SETUP

Figure 3 depicts a top-down view of the experimental apparatus. Components depicted in solid curves and lines represent elements common both to optical spectroscopy in hydrogen and neutron counting in deuterium. Within the chamber, this included only the electrode arrangement, for which the anode was the chamber itself (a stainless steel, vertically oriented cylinder of inner radius 24 cm) and the cathode which was a horizontally oriented, open-ended and stainless steel cylinder of length 4 cm, radius 1 cm, and steel thickness 3 mm.

Details of the high-voltage (HV) connections were changed with respect to our previous paper, with an emphasis on minimizing the exposure of connectors to the plasma (thereby minimizing arcing) by enclosing the connectors in ceramic. This allowed the dc discharge to be operated at parameters relevant to neutron production (tens of kV and tens of mA). Current and voltage are typically observed to vary only 5–10 % over 10–60 min intervals, and so the discharge is effectively steady-state with respect to the 30 s time scales of our spectroscopic measurements.

The cathode sat about 10 cm from the floor of the chamber and about 30 cm beneath a removable stainless steel x-ray shield. The cathode was oriented such that the axis of the highly collimated emission channels (labeled “beam axis” in the figure) would not impinge on the vacuum port or the spare HV feed, the latter of which was not used in the present work.

An external dc power supply (not shown) provided a cathode voltage of units to tens of kV at currents of units to tens of mA. Voltage, current and gas pressure were all measured directly—voltage using a HV probe across the electrodes, current using a gauge on the power supply, and absolute

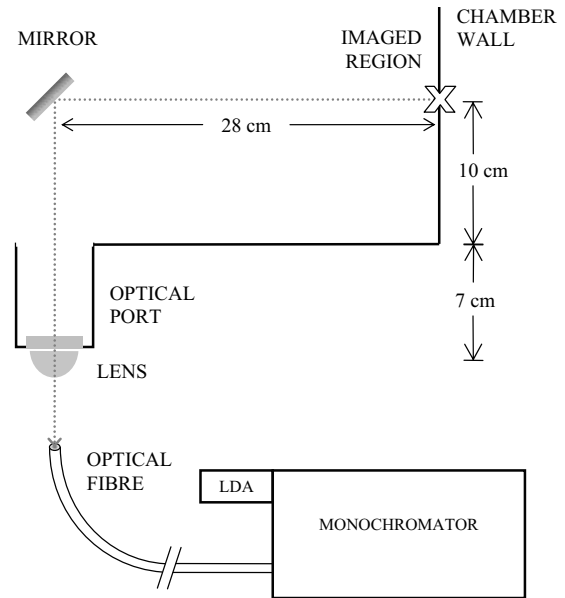


FIG. 4. Side-on schematic of the mirror, lens, and fiber optic arrangement used to sample light from the beam.

pressure using a Pirani gauge accurate to 10^{-4} Torr. Experimental error for each of these quantities is in the order 5%.

A. Optical spectroscopy in hydrogen gas

Optical spectroscopy in hydrogen was performed by sampling light from the beam in the region marked “X” in Fig. 3. That is, light was sampled at an angle $\theta \sim 30^\circ$ to the region where the beam struck the chamber wall, with the observation axis represented by the dotted line in the figure. These measurements made use of a back-coated mirror which was affixed to the interior (vacuum) side of a quartz optical port so that light from region X was channeled by the mirror down through the port. This arrangement is represented by the dotted circle in Fig. 3 and is shown in side-on schematic form in Fig. 4.

We note that the plane of the mirror was rotatable with its normal vector moving through a hemispherical range of azimuthal and inclination angles. The mirror was aligned by first running the IEC discharge at nominal parameters (25 kV and 30 mA at a pressure 5 mTorr) and burning a hole of radius ~ 1 cm through a sheet of aluminium foil affixed to the anode wall. For the calculations of Sec. IV, the radius of this hole serves also as an estimate of the neutral beam radius. Our mirror setup was able to image the entire diameter of this hole, and so we assume collection of light across the entire cylindrical cross sections of neutral and electron beams.

Subsequent to the mirror alignment procedure, light exiting the optical port was focused by a lens of focal length ~ 5 cm onto an optical fiber of effective width 1.25 mm. The total distance of the imaged region X to the centre of the converging lens was about 47 cm (see Fig. 4). Light exiting the fibre was channeled onto the slit of a 0.5 m focal length Spex 500M monochromator coupled to a Princeton Applied Research 1421G linear diode array (LDA) which was cooled

to 0 °C by a Peltier cooler in order to reduce thermal noise. The resolution of the detection setup was ~ 0.56 Å, determined by shining a cadmium lamp on region X and observing full widths at half maximum for the three strongest atomic emission lines in the wavelength range 6300–6500 Å. We calculated a wavelength separation 0.16 ± 0.01 Å between adjacent pixels of the output across the entire LDA. Optimal balance between signal strength and resolution was obtained for a monochromator slit width 250 μm .

B. Detection of neutron production rates in deuterium gas

For measurement of neutron production rates, the detector setup consisted of a ~ 1 cm² Li-I crystal, highly enriched with ⁶Li and housed within the center of a high density polyethylene sphere (shown by the shaded circle in Fig. 3). The 2.45 MeV neutrons produced in process 1 were slowed by the polyethylene sphere leading to the nuclear reaction



where product He nuclei scintillated the crystal producing a pulse of current on a photomultiplier. Output was read on a multichannel analyzer (MCA) allowing selection of the peak corresponding to 5 MeV α particles produced through process (8).

For each separate instance of pressure, current and voltage, neutron detection events were counted for 1–2 min with the error taken to be the statistical error (square root of the number of counts). These arbitrary detection rates were transformed into absolute neutron production rates by comparing the counts (per two minute period) to those observed at distances 20–100 cm from an Am-Be source of known activity ($\sim 10^6$ s⁻¹). In our calculations we assumed an average separation of 38 ± 4 cm between the detector and the beam source (see Fig. 4), a distance for which the Am-Be source yielded 1100 ± 200 counts in 2 min.

We note that as the mean free path for D-D fusion is very large (in the order 10^{12} m for 15 keV deuterons in a 5 mTorr deuterium gas), the density of energetic nuclei would have been largely constant along the beam axis, with neutrons produced at all points along the beam. As such we also expect some systematic error (15–20 %) in absolute counts due to the variation of detector distance from the extended source. This was generally less significant than the statistical error.

III. THEORY

A. Optical diagnostic for absolute densities of fast H ion species in H₂

Our spectroscopic method [3] implicitly calibrates the detector by relating the intensity ratios of Doppler-shifted (Gaussian) and central (Lorentzian) H_α peaks measured at the anode several centimeters away from the cathode and at an angle $\theta < 90^\circ$ to the beam, to the densities of fast and slow excited H also at the anode. The density of fast excited H at the anode is related to their density at the cathode by radiative decay constants, and subsequently to the densities

of fast ions emerging from the cathode through known charge-exchange rate coefficients. Similarly, we relate densities of slow H and fast electrons at the anode using rate coefficients for dissociative excitation by electrons.

In our previous paper the optical setup could only sample part of the beam cross sectional areas, and so the emission volumes associated with electron and neutral beams were equal. In this work however, the optical system samples the entire cross sectional area of both beams (which may take different radii) and so we must make a correction to the right-hand side of our original expression by incorporating the factor $(r_e/r_n)^2$. That is, we expect a given peak intensity to be proportional both to the number density of emitting particles, and the corresponding emission volume (beam area). We need apply no other spatial or wavelength-related corrections to the peak intensity ratios, as they are recorded in the same spectrum and in the same region of space. The result is a single expression relating intensity ratios to the ratio of ion and electron densities

$$f_{\text{fast}} = \frac{n_{\text{H}_x^+}^{\text{cathode}}}{n_{\text{H}_2}} = \frac{n_{e_{\text{fast}}}^{\text{anode}} r_e^2}{n_{\text{H}_2} r_n^2} \frac{I_x^{\text{anode}}}{I_{\text{central}}^{\text{anode}}} \frac{\sigma_{\text{DE}}(n=3) v_{e_{\text{fast}}}^{\text{anode}}}{\sigma_x(3s) v_{\text{H}_x^+}^{\text{cathode}}} \times [(1 + C_1) C_2 \exp(-A_{3s \rightarrow 2p} t_{\text{sep}})]^{-1}, \quad (9)$$

where f_{fast} is the dissociation fraction of the background gas into energetic nuclei, $n_{\text{H}_x^+}^{\text{cathode}}$ is the number density (units m³) of fast H_x^+ of velocity $v_{\text{H}_x^+}^{\text{cathode}}$ in the vicinity of the cathode edge, $n_{e_{\text{fast}}}^{\text{anode}}$ is the number density of fast, monoenergetic electrons of velocity $v_{e_{\text{fast}}}^{\text{anode}}$ at the anode, and n_{H_2} is the density of the background gas. I_x^{anode} is the intensity (arbitrary units) of Doppler emission arising from fast H_x^+ and measured at an angle θ to the emission channel at the anode, whereas $I_{\text{central}}^{\text{anode}}$ is the central peak intensity including Doppler shifts up to 0.3 Å from the unshifted wavelength.

The cross section $\sigma_x(3s)$ (units m²) is for the branch of charge exchange of fast H_x^+ resulting in fast atomic H(3s) at the cathode edge, whereas $\sigma_{\text{DE}}(n=3)$ is for the branch of dissociative excitation of H₂ by fast electrons producing slow H($n=3$) at the anode. $A_{(nl) \rightarrow (n'l')}$ is the Einstein coefficient (s⁻¹) for an optically allowed transition H($nl \rightarrow n'l'$), and t_{sep} is the time-of-flight for fast H(3s) traversing the distance (~ 24 cm) from cathode-to-anode (having energy $1/x$ of the incident fast H_x^+). The constants C_1 and C_2 are defined as

$$C_1 = \frac{0.44A_{3p \rightarrow 1s}}{(0.16A_{3s \rightarrow 2p} + 0.44A_{3p \rightarrow 2s} + 0.40A_{3d \rightarrow 2p})}, \quad (10)$$

$$C_2 = \frac{A_{3s \rightarrow 2p}}{[A_{3s \rightarrow 2p} + n_{\text{H}_2} \sigma_Q(3s) v_{\text{H}(3s)}]}, \quad (11)$$

where $\sigma_Q(3s)$ is the cross section for radiationless collisional deexcitation (“quenching”) of fast H(3s).

It has been shown [10,11] that for pressures in the tens of mTorr range, the Doppler peaks associated with fast H_2^+ and H_3^+ are not resolved but instead form a merged peak. Moreover these species are expected to be present in approxi-

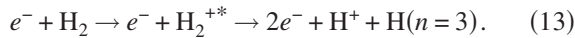
mately equal numbers [6], and so for this peak (referred to in our results section as “fast $H_{2.5}^{+}$ ”) we assume an average incident ion mass corresponding to $x=2.5$. As a result, we take the cross section for Doppler emission to be the average of total H_α production by fast H_2^+ and H_3^+ in H_2 [13] which we then divide by three to specify fast H produced in the $3s$ state. We thus have $\sigma_{x=2.5}(3s)=5.0 \times 10^{-22} \text{ m}^2$. We divide also the $n=3$ quenching cross section of Ref. [14] in the same way, yielding $\sigma_Q(3s)=7.4 \times 10^{-19} \text{ m}^2$. Both of these cross sections are taken to be constant for interactions in the tens of keV energy range. Experimental cross sections for dissociative excitation in the tens of keV range do not exist, and so we use the high-energy Born-fit quoted by Janev *et al.* [15]; for 30 keV electrons we have $\sigma_{DE}(n=3)=3.0 \times 10^{-24} \text{ m}^2$. Values for the Einstein emission coefficients (averaged over fine transitions and assuming no field-induced mixing effects) were obtained from Wiese *et al.* [16].

With regards to the electron densities, for a cylindrical beam of fast and approximately monoenergetic electrons (charge e and mass m_e) with constant flux and radius r_e , the density of electrons as a function of their velocity v_e and cathode current I_{cathode} is given by

$$n_{e_{\text{fast}}}^{\text{anode}} = I_{\text{cathode}} / (\pi r_e^2 e v_{e_{\text{fast}}}^{\text{anode}}), \quad (12)$$

where the velocity of electrons at the anode assumes they are accelerated from rest to the full applied potential [8], with relativistic effects neglected.

Certain atomic emission processes are able to be neglected in this analysis. One is dissociative ionization of H_2 by electrons



This process, while likely playing a role in sustaining the discharge, produces H_α with Doppler shifts $0.5 \leq |\Delta\lambda| \leq 3 \text{ \AA}$ [7] which are larger than our chosen definition of the central peak. Assuming that the density of ground state atomic H is much smaller than for H_2 , we can neglect also electron excitation of atomic H.

B. Prediction of neutron production rates in deuterium

The key claim in this work is that we may use the dissociation fraction at the cathode edge (f_{fast}) measured in hydrogen to predict the volumetric neutron production rate R_{vol} ($\text{m}^{-3} \text{ s}^{-1}$) of process (1) for a deuterium discharge which has the same cathode current and voltage. We term this an “equivalent” discharge of D_2 . We anticipate that the values f_{fast} and R_{vol} are related through

$$R_{\text{vol}} = n_{D_x} n_{D_2} (2x\sigma_{D-D}) v_{D_x} = 2x f_{\text{fast}} (n_{D_2})^2 \sigma_{D-D} v_{D_x}, \quad (14)$$

where n_{D_x} is the population density of fast monoenergetic deuteron nuclei at the cathode edge, with mass x times that of a single deuteron and velocity v_{D_x} .

We note that n_{D_x} refers primarily to the neutral population, as in our model fast ions have largely been neutralized beyond the cathode. The density of deuterium gas is given by n_{D_2} , with σ_{D-D} the cross section for neutron production by

process (1). We use the cross sections quoted in Ref. [17], multiplying them by a factor $2x$ to account for the increased density of nuclei in the reaction between fast D_x and the gas molecule D_2 . For the setup in Fig. 3, we assume each beam of energetic deuterons to be cylindrical with radius $r_n = 1 \text{ cm}$ and length $L=24 \text{ cm}$. Thus the total absolute neutron production rate R_{tot} (s^{-1}) for the system is given by

$$R_{\text{tot}} = (2L\pi r_n^2) R_{\text{vol}}. \quad (15)$$

Combining Eqs. (9), (12), (14), and (15) we see that the absolute neutron production rate is independent of the electron and neutral beam radii, however, the error in f_{fast} and R_{vol} is dominated by the uncertainty in these quantities.

C. Uncertainty associated with predicted fusion rates

In our previous paper [3], the optical method encompassed here by Eqs. (9) and (15) was associated with an order-of-magnitude error, dominated by the uncertainty in particle velocities, densities, and atomic interaction cross sections which arise from the assumption of monoenergetic electrons and ion species. Here we assess newly identified uncertainties inherent in these expressions, extending the corresponding analysis from our previous paper and further justifying this error estimate.

Williams *et al.* [18] show that similar to fast electrons, fast H and H_x^+ at units and tens of keV energies may produce slow $H(n=3)$ by dissociative excitation of hydrogen gas, and that the cross section for these processes are similar to the corresponding production of fast $H(3s)$. For central peak emission at the anode, we may neglect any contribution from H_x^+ as ion energies at the anode are low. However, we cannot similarly discount the component of central peak emission arising from fast neutral H, as this should exhibit intensities comparable to the Doppler shifted peaks. In fact for H energies of 5–15 keV the production ratio of fast $H(3s)$ to slow $H(n=3)$ is 1.2 ± 0.1 which is about 40–50 % of the corresponding Doppler to central-peak intensity ratios we measure in Sec. IV A. As such Eq. (9) may be overestimating the component of central peak emission due to electron excitation by as much as 50%.

We have neglected electric field mixing in the production of fast $H(3s)$ at the cathode and slow $H(n=3)$ at the anode. This is justified as we expect the electric field in both of these regions to be small—in our model the cathode edge exhibits a local potential minimum, and we assume the anode to sit sufficiently beyond the cathode fall. We note, however, that in the cathode fall region we anticipate axial fields exceeding 1 kV/cm, and this may decrease the $3s$ lifetime by an order of magnitude (see Fig. 9 of Ref. [19]). Taking this effect into account would require careful modification of the assumed $H(3s)$ decay [as given by Eq. (8) of our previous paper], and we acknowledge it as a shortcoming here.

Strictly speaking Eq. (15) requires a sum over all the fast ion species x . However, for the measurements in Sec. IV A we have focused only on the Doppler peak corresponding to fast $H_{2.5}^+$ as the fast H^+ peaks were not always visible (intensities for H^+ Doppler peaks were generally less than 10% of those for $H_{2.5}^+$). However, neglecting the contribution of

H^+ in this way may underestimate the predicted fusion rate by up to an order of magnitude as the fusion cross sections for these more energetic nuclei are about an order of magnitude larger. We have similarly neglected any contribution to fusion rates by fast neutral particles reflecting from the anode surface which, as evidenced by the corresponding Doppler shifted emission in Fig. 6, may not be insignificant. Equation (15) for the total fusion rate also ignores any fusion reactions for fast deuterium nuclei accelerating from the cathode center towards the cathode interior wall; this is justified on the grounds that the cathode interior comprises only a small fraction ($<10\%$) of the total fusion reaction volume in the system.

It is also possible that cathode heating may influence the temperature and density profile of the gas, whereas our model assumes uniform profiles for both. Experimentally, we have attempted to minimize this issue by allowing the cathode to cool (switching off the discharge) between individual measurements of H_α spectra and neutron production rates.

Given the numerous sources of error in our expressions as presented here, we conclude that any single theoretical prediction of fusion rate is associated with an order-of-magnitude uncertainty at best.

IV. RESULTS AND DISCUSSION

This section is comprised of two subsections. The first details the measurement of H_α Doppler- and central-peak emission intensities for the cases of constant pressure and voltage in the IEC apparatus of Sec. II. In the second, we measure neutron counts in D_2 , comparing them to predictions obtained from the measurements in hydrogen and demonstrating the validity of the diagnostic.

A. Measurement of central- and Doppler-peak intensities in H_2

1. Constant voltage

Keeping the cathode voltage constant at -30.0 ± 0.5 kV and with cathode currents in the range 1–30 mA, we recorded several H_α spectra at an angle $\theta=30^\circ$ to the emission channel as described in Sec. II A. Cathode current was varied by adjusting hydrogen gas pressure in the range 4–6 mTorr, with the variation of pressure with current shown in Fig. 5. For this condition we carried out three trials, grouped by the three shapes (squares, triangles, and circles) of hollow data points in the figure. Each separate trial exhibits a rapid increase of current with pressure, and demonstrates the difficulty in replicating a particular set of plasma parameters in any two trials.

We recorded fifteen spectra across the three trials in hydrogen. For each spectrum the total accumulation time was typically 30 s, summed over 7–15 shorter exposures. Our method does not require a constant exposure time and so this was adjusted to obtain the best signal; for 20–30 mA a maximum accumulation time of 30 s was appropriate as it proved difficult to maintain the discharge for longer than this. Figure 6 shows a spectrum recorded at -30 kV and 27 mA.

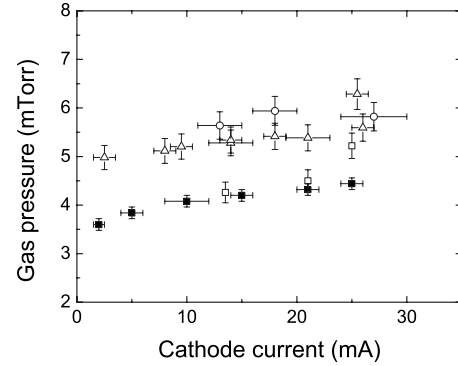


FIG. 5. Pressure versus cathode current (cathode voltage -30 kV). Hollow data points represent separate experimental runs in hydrogen, whereas solid points are for deuterium.

The total intensity of Doppler redshifted emission is clearly greater than for the blueshifted wing, with the red peak also extending out to larger Doppler shift magnitudes, suggesting that fast $H(3s)$ at the imaged region X (see Fig. 3) travel primarily towards the anode wall. The central peak intensity is associated with the area under the Lorentzian fitted using a commercial software package (ORIGIN). The shaded part of the central peak corresponds to the region where $|\Delta\lambda| \leq 0.3 \text{ \AA}$. Following the procedure in Refs. [3–6,10], intensities due to charge exchange processes are associated with the area under Gaussians fit to energetic Doppler peaks.

As explained in Sec. III A and in Ref. [3], we are concerned with the redshifted peak “fast $H_{2.5}^+$ ” (the shaded Gaussian in Fig. 6) due to incident fast $H_{2.5}^+$ of average mass $2.5 \times m_H$. We have also labeled redshifted and blueshifted peaks which may arise from a combination of lower-energy (tens and hundreds of eV) secondary ions produced in reactions (5)–(7) as well as projectile excitation of fast H reflected at various angles off the anode wall. We identify also a redshifted peak for fast H^+ , however, this peak was not always visible for the lower-current (noisier) spectra.

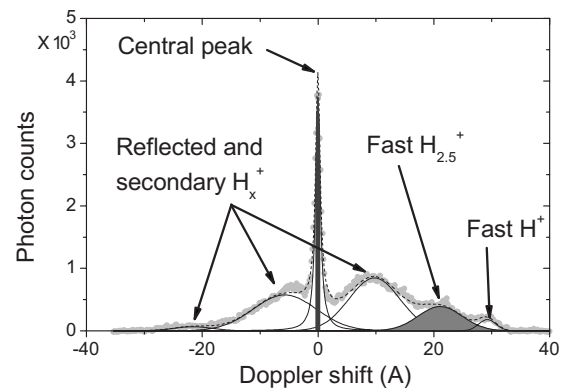


FIG. 6. Typical H_α spectrum (discrete points) observed at $\theta=30^\circ$ to the emission channel at the anode wall (constant voltage of -30 kV). We label the Lorentzian fitted to the central peak as well as Gaussians for redshifted and blueshifted Doppler peaks. The dashed curve represents the total fit. Shaded regions are explained in the text.

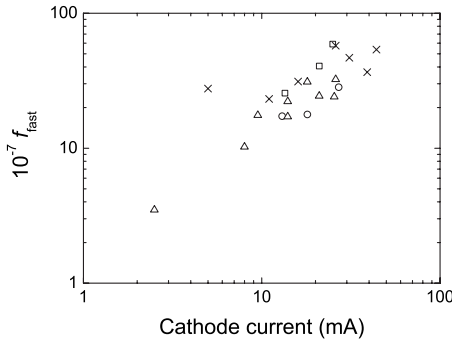


FIG. 7. Dissociation fractions f_{fast} measured for constant voltage (three sets of hollow data points corresponding to different experimental trials as in Fig. 5) and constant pressure (crosses, corresponding to the same symbols in Fig. 2).

Incident $\text{H}_{2.5}^+$ are assumed to be approximately monoenergetic, their energies determined using Eq. (3) with the observed Doppler shift $\Delta\lambda$ for a given peak maximum. For the constant voltage condition, the fast $\text{H}_{2.5}^+$ were found to have incident mean energy 51% of the applied cathode potential (standard deviation 5%). This is reminiscent of other spectroscopy results near and within our current range but for different cathode geometries, for example, Ref. [3] featuring a segmented cylindrical cathode (typically 50–60% of the applied potential) and Refs. [4,5] featuring a “three-ring” spherical grid (~20–25%).

Intensities for the central and fast $\text{H}_{2.5}$ peaks were found to exhibit a linearlike increase with current over the 1–30 mA range, however, the ratio $I_x^{\text{anode}}/I_{\text{central}}^{\text{anode}}$ of Doppler-to central-peak emission showed no such systematic variation, with a mean of 2.5 ± 0.7 (where we have defined the uncertainty as one standard deviation across the fifteen spectra). By equating the two right-hand side lines of Eq. (9), the average ratio of densities for fast $\text{H}_{2.5}^+$ (or equivalently, fast $\text{H}_{2.5}$ nuclei) at the cathode edge to fast electrons at the anode was 72 ± 17 , also showing no clear dependence on current. We note that this is about 50% smaller than the corresponding density ratio in our previous paper. We suspect this may be due to slight differences in the cathode geometries; the cathode in the previous paper was a segmented cylinder with only half the steel thickness of our present cathode, which may increase the heating, secondary electron emission rates and thus ion densities within the cathode.

Dissociation fractions f_{fast} were calculated using Eq. (9) and are shown by the hollow data points in Fig. 7. These correspond to the three constant voltage (–30 kV) trials in Fig. 5, and suggest a linearlike increase of f_{fast} from $5\text{--}30 \times 10^{-7}$ for currents 5–30 mA. We note that values of f_{fast} are associated with an order of magnitude uncertainty due to the range of possible electron and neutral beam radii, with variations up to 50% between trials also demonstrating the difficulty in replicating particular experimental conditions. The corresponding densities for energetic $\text{H}_{2.5}^+$ at the cathode edge show a similarly linear dependence on current over this range, increasing from $1\text{--}6 \times 10^{14} \text{ m}^{-3}$.

2. Constant pressure

The measurements from Sec. IV A 2 were repeated for a single trial of constant hydrogen gas pressure ~4 mTorr,

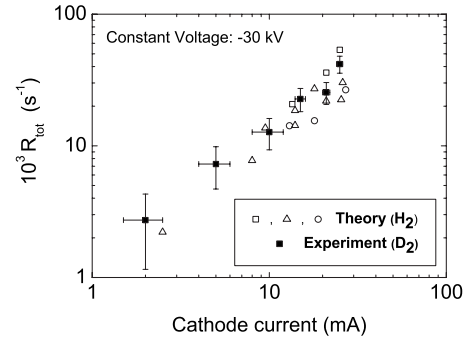


FIG. 8. Solid data points represent measured neutron counts for the conditions of constant voltage (–30 kV) in deuterium. Hollow data points show the values predicted using Doppler spectroscopy in hydrogen.

with cathode voltage 15–25 kV and currents in the range 1–45 mA. A plot of voltage versus current is shown by the cross data points in Fig. 2. We recorded seven spectra with exposure and accumulation times typical of the constant voltage measurements. Here the fast $\text{H}_{2.5}^+$ were found to have incident mean energy $49 \pm 3\%$ of the applied cathode potential, and as with the constant voltage spectra the ratio $I_x^{\text{anode}}/I_{\text{central}}^{\text{anode}}$ takes a largely unchanging value of 2.6 ± 0.8 for the six spectra in the current range 10–30 mA. The average ratio of densities for fast $\text{H}_{2.5}$ nuclei at the cathode edge to fast electrons at the anode was 73 ± 20 , except for the lowest current spectrum (5 mA) which had a ratio of ~210.

The dissociation fractions f_{fast} for the constant pressure condition are shown by the cross data points in Fig. 7. We observe an increase from $2\text{--}6 \times 10^{-6}$ for currents 10–45 mA, in fact for currents 10–30 mA the dissociation fractions for the constant pressure and voltage conditions are in agreement to within about 50%. Corresponding densities for energetic $\text{H}_{2.5}^+$ at the cathode edge increase in a similar fashion from $4\text{--}9 \times 10^{14} \text{ m}^{-3}$ across the 10–45 mA range.

B. Measured and predicted neutron production rates in D_2

Following the procedure in Sec. II B, the solid data points in Fig. 8 show the total neutron production rates for the case of constant voltage (–30 kV) in the experimental discharge of deuterium, which exhibit a linearlike increase from $1\text{--}4 \times 10^4 \text{ s}^{-1}$ for currents 10–30 mA. The hollow points in the figure show values of R_{tot} predicted using the H_2 dissociation fractions obtained in Sec. IV A 1. Similarly, the solid data points in Fig. 9 show the total measured neutron production rates for the case of constant pressure (6 mTorr) in D_2 , with the H_2 predictions (see Sec. IV A 2) represented by crosses. Here the current dependence is less linear, which is to be expected as the voltage (and thus deuteron energy and fusion cross section) varies with current.

In both experimental conditions, the predicted and measured absolute rates agree to within an order of magnitude, with predicted rates also capturing the current dependence of the observed neutron production. The agreement between predicted and measured rates is best between 10–20 mA for

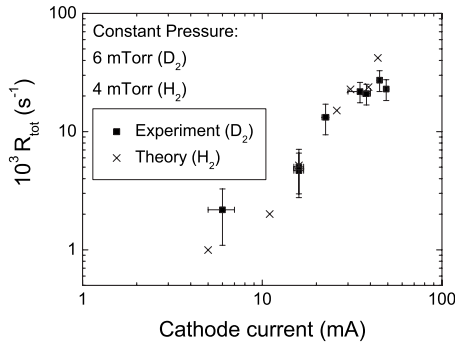


FIG. 9. Solid data points represent measured neutron counts for the conditions of constant pressure (6 mTorr) in deuterium. Hollow data points show values predicted using Doppler spectroscopy in hydrogen.

the constant voltage data, and between 15–40 mA for constant pressure. A divergence in the order 50% at lower currents may correlate to a change of the discharge mode from an abnormal to normal hollow cathode discharge as current decreases (Fig. 2). Similar divergence for larger currents (and in particular between separate trials of constant voltage) correlates to increased arcing and larger intensity variations at the upper end of our current range.

We note that in Eq. (14) for the volumetric neutron production rate, we assumed that neutral particles comprised the majority of fast nuclei emerging from the cathode apertures. If the dominant species were ions, then the equivalent form of Eq. (15) would require an integral over position-dependent functions of ion velocity and neutron production

cross section, the product of which would decrease over several orders of magnitude with increasing distance from the cathode. This would leave neutron production only to those fast ions in the vicinity of the cathode edge, reducing the reaction volume by at least an order of magnitude and thus the predicted fusion rates as well. As a result, the good agreement between predicted and observed neutron production rates in the 10–40 mA current range appears to support our present model of the abnormal hollow cathode discharge, where the majority of fast nuclei are neutral particles emerging from the cathode apertures.

V. CONCLUSIONS

We have demonstrated the applicability of the optical diagnostic from Ref. [3] to the highly collimated and cylindrically symmetric IEC (abnormal hollow cathode) hydrogen discharge described in Sec. II A. This was achieved by measuring dissociation fractions f_{fast} of H_2 gas and using these to predict absolute neutron production rates for equivalent discharges of D_2 , under the separate conditions of constant pressure and voltage. The good agreement (generally to within an order of magnitude) between measured and predicted neutron production rates supports the model of Ref. [10] for the abnormal hollow cathode discharge, in which the majority of energetic neutrals emerge from the cathode apertures. Moreover, we have shown that in the abnormal hollow cathode regime and where voltage is kept constant, f_{fast} is proportional to the cathode current—we expect that this will prove useful in predicting the neutron production rates for even larger currents.

-
- [1] R. L. Hirsch and G. A. Meeks, U.S. Patent No. 3,530,497, 1970.
- [2] K. Noborio, T. Sakai, and Y. Yamamoto (unpublished).
- [3] J. Kipritidis, J. Khachan, M. Fitzgerald, and O. Shrier, Phys. Rev. E **77**, 066405 (2008).
- [4] J. Khachan and S. Collis, Phys. Plasmas **8**, 1299 (2001).
- [5] J. Khachan, D. Moore, and S. Bosi, Phys. Plasmas **10**, 596 (2003).
- [6] M. Fitzgerald, J. Khachan, and S. Bosi, Eur. Phys. J. D **39**, 35 (2006).
- [7] G. Baravian, Y. Chouan, A. Ricard, and G. Sultan, J. Appl. Phys. **61**, 5249 (1987).
- [8] J. Kipritidis, M. Fitzgerald, and J. Khachan, J. Phys. D **40**, 5170 (2007).
- [9] G. McClure, Phys. Rev. **140**, A769 (1965).
- [10] O. Shrier, J. Khachan, S. Bosi, M. Fitzgerald, and N. Evans, Phys. Plasmas **13**, 12703 (2006).
- [11] O. Shrier, J. Khachan, and S. Bosi, J. Phys. A **39**, 11119 (2006).
- [12] J. Khachan and A. Samarian, Phys. Lett. A **363**, 297 (2007).
- [13] A. Phelps, J. Phys. Chem. Ref. Data **19**, 653 (1990).
- [14] M. Wouters, J. Khachan, I. Falconer, and B. James, J. Phys. B **32**, 2869 (1999).
- [15] R. Janev, W. Langer, K. Evans, and J. D. E. Post, *Elementary Processes in Hydrogen-Helium Plasmas* (Springer-Verlag, Berlin, 1987).
- [16] W. Wiese, M. Smith, and B. Glennon, *Atomic Transition Probabilities. Hydrogen Through Neon. A Critical Data Compilation*, NSRDS-NBS 4 (U.S. Department of Commerce, National Bureau of Standards, Washington, D.C., 1966).
- [17] C. F. Barnett, J. A. Ray, E. Ricci, M. I. Kirkpatrick, E. W. McDaniel, E. W. Thomas, and H. B. Gilbody, *Atomic Data for Controlled Fusion Research Volume II* (Controlled Fusion Atomic Data Center, Oak Ridge National Laboratory, Oak Ridge, TN, 1980).
- [18] I. Williams, J. Geddes, and H. Gilbody, J. Phys. B **15**, 1377 (1982).
- [19] C. C. Havener, N. Rouze, W. B. Westerveld, and J. S. Risley, Phys. Rev. A **33**, 276 (1986).